Near-inertial oscillations interacting with mesoscale circulation in the southwestern Japan/East Sea

Jae-Hun Park and D. Randolph Watts

Graduate School of Oceanography, University of Rhode Island, Narragansett, Rhode Island, USA

Received 9 March 2005; revised 15 April 2005; accepted 21 April 2005; published 24 May 2005.

[1] The near-inertial internal wave energy distribution is investigated in the southwestern Japan/East Sea using vertical round-trip travel time of sound (τ) data from 23 pressure-sensor-equipped inverted echo sounders (PIESs) and data from Aanderaa recording current meters (CMs). Currents associated with low-mode near-inertial internal waves are slightly inclined and displace the thermocline vertically, which can be detected in τ. The band-pass filtered τ records exhibit high near-inertial energy distributions that vary interannually with changes observed in mesoscale circulation. An explanation for this is offered as trapping of near-inertial energy in anticyclonic regions, which is supported by scatterplots of monthly-rms band-pass filtered τ at inertial frequency bands vs. monthly-mean relative vorticity. The spectra from all but one deep CM exhibit a blue shift, consistent with the equatorward propagation of near-inertial waves. The exception has the highest near-inertial wave energy, and is located near the center of a warm anticyclonic eddy. **Citation:** Park, J.-H., and D. R. Watts (2005), Near-inertial oscillations interacting with mesoscale circulation in the southwestern Japan/East Sea, *Geophys. Res. Lett.*, *32*, L10611, doi:10.1029/2005GL022936.

1. Introduction

[2] Near-inertial oscillations in the open ocean are internal waves with a frequency close to the Coriolis frequency f. Because the internal wave band supports frequencies $f \leq \omega \leq N$, where N is buoyancy frequency, freely propagating near-inertial oscillations are restricted to frequencies higher than the local f.

[3] Recently, *Garrett* [2001] emphasized a unique behavior of near-inertial waves, which propagate equatorward along a slanted ray path which steepens as f decreases. Hence, their energy arrives at the ocean bottom equatorward of the source region. He supported his theory with examples from *Fu* [1981] that show the frequency of near-inertial oscillations increases with the depth, and he commented on the need for a reappraisal of internal wave theories with an increased emphasis on the near-inertial band.

[4] However, as *Garrett* [2001] mentioned, his theory ignored the effect of current shear that refracts and may trap the near-inertial wave energy. This interaction was the subject of several studies [e.g., *Kunze*, 1985]. *Kunze* [1985] showed that near-inertial wave energy can be trapped in a region of negative relative vorticity ($\zeta < 0$), which creates a waveguide by shifting the lowest internal wave frequency from f to an effective Coriolis frequency $f_{\text{eff}} = f + \zeta/2 < f$.

[5] Near-inertial motions in the upper ocean are dominated by nearly horizontal oscillating currents because the value of the ray angle (α) of near-inertial waves is O(10^{-3}) rad, where α is between the wave number vector and the horizontal. However, even with this tiny α, the near-inertial oscillations in the thermocline can produce a vertical displacement of the thermocline, which changes τ measurably [*Watts and Rossby*, 1977]. *D'Asaro* [1991] shows that low-mode near-inertial waves can propagate as much as O(2000 km) equatorward. In his simulation, the near-inertial waves in the thermocline even 2000 km south of a storm have speeds of about 1 cm s^{-1} and vertical displacements of about 1 m for the subsequent 20 days.

[6] In this paper, we utilize the mapped mesoscale circulations, for which the moored measurements were originally designed, in an innovative and unanticipated way: To investigate their impact on near-inertial wave energy distribution in the upper and deep southwestern Japan/East Sea. The upper inertial oscillations were observed using the vertical round-trip travel time of sound (τ) records collected by pressure-sensor-equipped inverted echo sounders (PIESs). The deep inertial oscillations were measured by Aanderaa recording current meters (CMs).

2. Data and Methods

[7] Twenty-five PIESs with 55–60 km spacing to cover the southwestern Japan/East Sea, which is called the Ulleung Basin (UB), were deployed from June 1999 to July 2001 (Figure 1). The PIES measured hourly τ with 0.05 ms accuracy. One PIES at P41 was lost, and P15 measured τ only for two months. Thus, we use 23 data sets of hourly τ in this study. Every data set has 17712 values from 0100 UTC 16 June 1999 to 0000 UTC 23 June 2001. The τ data set is analyzed with a band-pass filter (4th-order Butterworth) to investigate temporal changes of near-inertial wave energy. The cutoff of the band-pass filter is $\pm$1.75 hours from the inertial period of each PIES site. The filtering is carried out in the forward direction, and then the filtered sequence is reversed and run again through the filter in order to eliminate all phase shifts. Using the band-pass filtered results, τ_i, we produce wintertime-mean (from November 1 to March 31) horizontal maps of near-inertial wave energy distribution.

[8] The 5-day low-pass filtered τ records additionally provide proxy estimates of the vertical profiles of temperature (T) and specific volume anomaly (δ). *Park et al.* [2005] estimated 2-year three-dimensional daily time series of T and δ using multi-indexed lookup tables. By mapping

0094-8276/05/2005GL022936$05.00

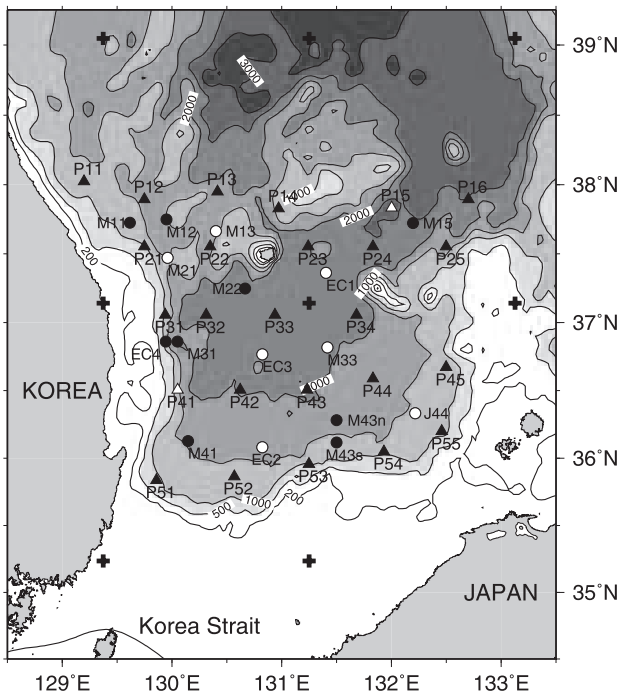

Figure 1. The southwestern Japan/East Sea. Triangles and circles indicate PIES and CM sites (solid marker sites are used in this study). Pluses represent NCEP wind stress data points. Bathymetry contours are in meters.

the depth of the 5°C isotherm, Z_5, using the time series of T fields, we examine the circulation patterns in the UB. An analogous investigation of the interaction between the internal tides and mesoscale circulation was reported by J.-H. Park and D. R. Watts (Internal tides in the southwestern Japan/East Sea, submitted to Journal of Physical Oceanography, 2005). By mapping the relative vorticity of the surface circulation, ζ, using the time series of δ fields, we examine the effects of ζ on the near-inertial internal wave energy distribution.

[9] For the qualitative comparison between near-inertial internal wave energy distribution and mesoscale circulation, we estimated monthly-rms τ_i and monthly-mean ζ at all 9 PIES sites, which were located away from the edges of our observation domain such that the mapping errors for ζ were relatively small. We divided the time series of τ_i and ζ into successive 30-day segments stepped at 15-day interval (50% overlap).

[10] Sixteen CMs were concurrently deployed at approximate midpoints between the PIESs. Hourly and one-half hourly current speed and direction data were collected by twelve and four CMs, respectively, at 20–40 m above the bottom (Figure 1). The eight major tidal constituents (M2, S2, N2, K2, K1, O1, Q1, and P1) were removed from the current records using a harmonic analysis technique. After that the one-half hour interval data were interpolated into hourly intervals. More details of the moorings and data processing of the PIESs and the CMs are given by *Mitchell et al.* [2005] and *Teague et al.* [2005].

[11] The CM records were divided into successive segments to calculate the power spectra of current using Welch's method, available in the Matlab toolbox. Each segment had 512 data points (21.33 days) long, and segments were overlapped by 50%. The CM could record a minimum current of 1.1 cm s^{-1}, and hence any value less than this was considered a current stall (little or no current). Some records had numerous stalls, requiring the following special treatment. When stalls occurred at less than 25% of the points in a segment, we calculated the unsmoothed spectral estimates of eastward (u) and northward (v) current components, and averaged the spectral estimates for all segments to produce smoothed spectral estimates with reduced error bars. For our study, we utilized only the CM records for which at least 20 segments contributed to the smoothed spectral average (solid circles in Figure 1).

[12] The NCEP/NCAR Reanalysis wind stress data ($\vec{\sigma}$) with 6-hour interval and 1.875 by 1.904 degree resolution were obtained from the NOAA-CIRES Climate Diagnostic Center for the 2 years of our observations (pluses in Figure 1).

3. Results

[13] Figures 2a and 2b exhibit time series of basin-averaged magnitudes of wind stress $\langle|\vec{\sigma}|\rangle$ in the UB (8 locations shown in Figure 1), and near-inertial currents $\langle U_i\rangle$ in the mixed-layer predicted from $\langle|\vec{\sigma}|\rangle$ using a

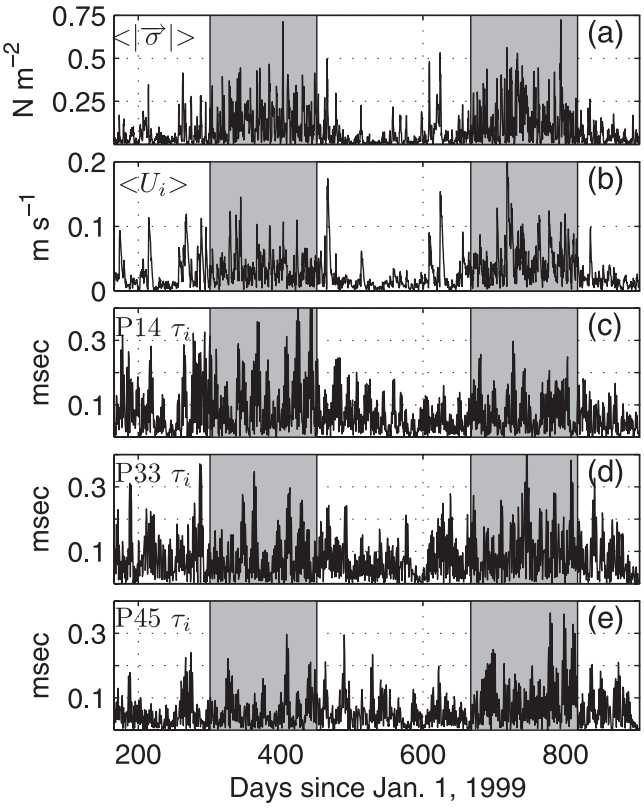

Figure 2. (a) Basin-averaged magnitude of wind stress $\langle|\vec{\sigma}|\rangle$. (b) Near-inertial currents in the mixed-layer $\langle U_i\rangle$, predicted from the $\langle|\vec{\sigma}|\rangle$ using a damped slab model. Amplitudes of band-pass filtered τ in the near-inertial frequency bands (τ_i) at sites (c) P14, (d) P33, and (e) P45. Gray shaded periods indicate the wintertime (November 1–March 31), during which the mean maps in Figure 3 are produced.

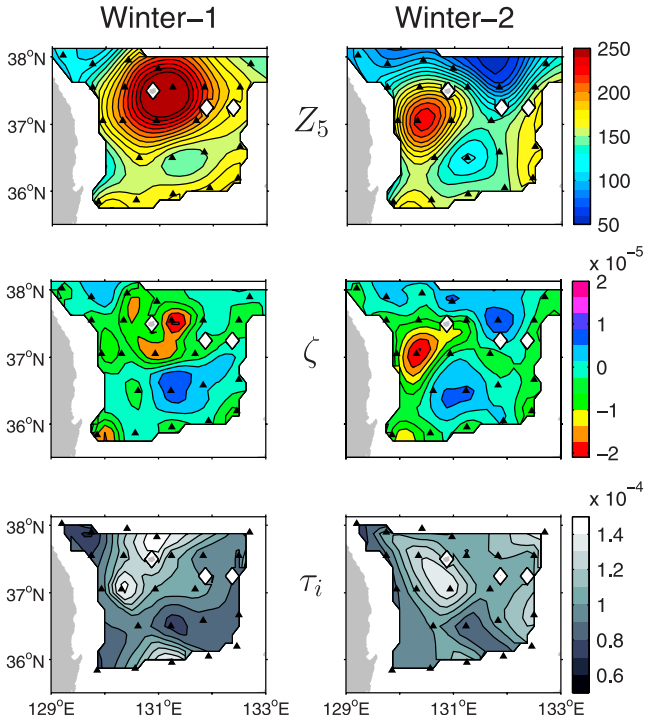

Figure 3. (top) Wintertime-mean maps of 5°C depth (Z_5) (contour interval 10 m). (middle) Relative vorticity (ζ) of the observed surface circulation (contour interval 4 × 10^{-6} s^{-1}). (bottom) Wintertime rms amplitude of band-pass filtered τ in the near-inertial frequency bands (τ_i) (contour interval 10^{-5} s). Winter-1 is from November 1, 1999 to March 31, 2000 (first column), and Winter-2 is from November 1, 2000 to March 31, 2001 (second column).

damped slab model [*D'Asaro*, 1985] with correction for the finite sampling interval of $\overrightarrow{\sigma}$ [*Niwa and Hibiya*, 1999]. The $\langle|\overrightarrow{\sigma}|\rangle$ and $\langle U_i\rangle$ time series reveal seasonal variations caused by the Asian Monsoon – stronger (weaker) $\overrightarrow{\sigma}$ during winter (summer) time.

[14] Figures 2c–2e exhibit time series of band-pass filtered τ at the inertial frequency band (τ_i) for three PIES sites (P14, P33 and P45). Interestingly, each time series of τ_i exhibits different seasonal variation. The τ_i at P14 shows higher values during Winter-1 (first gray-shaded period from November 1, 1999 to March 31, 2000) than during Winter-2 (second gray-shaded period from November 1, 2000 to March 31, 2001), while the τ_i at P45 shows higher values during Winter-2 than during Winter-1. The τ_i at P33 shows almost equal value during each winter. This inter-site variability led us to seek an explanation other than $\langle|\overrightarrow{\sigma}|\rangle$, possibly associated with the vorticity field of the mesoscale circulation.

[15] Figures 3(top) and 3(middle) exhibit maps of wintertime-mean circulation (5°C depth Z_5) and the corresponding relative vorticity of the surface circulation (ζ) during each winter. In the Winter-1 map, the Ulleung Warm Eddy (UWE) is strongly developed with diameter about 200 km. A branch of the Tsushima Warm Current (TWC) flows along the southern edge. The associated Winter-1 ζ map exhibits significant negative values near the strongly developed UWE core and along this southern edge. In the Winter-2 map, the UWE shrinks to a small eddy with diameter about 100 km. The TWC branch turns offshore (northward) along the eastern edge of the domain and the meandering Subpolar Front (SPF) shifted south of 38°N. The associated Winter-2 ζ map exhibits significant negative values near the shrunken UWE core and along the eastern edges.

[16] For each winter, Figure 3(bottom) maps the rms amplitudes of τ_i. The hot spots of near-inertial energy change locations between years, as we next relate to the circulation. At all the strong near-inertial energy spots, the wintertime-rms τ_i exceeds 0.13 ms during the two winters.

[17] Comparison with the Z_5 maps suggests a relationship between the near-inertial energy distribution and the mesoscale circulation. During Winter-1, when the UWE is strongly developed, strong near-inertial oscillations occur in the northern part of the UWE near the boundary between the UWE and the SPF and southern part of the UWE. Another high energy spot occurs near the southern edge near 131°E along the TWC branch. During Winter-2, the strong near-inertial oscillations shift southward near the center of the UB (37.5°N), again near the boundary between the UWE and the SPF. Another high energy spot occurs near the eastern edge along the TWC branch. Hence when the hot spots of near-inertial oscillations are viewed in relation to the circulation, they are found in analogous locations: The hot spots of near-inertial oscillations appear where the ζ maps are anticyclonic.

[18] Figure 4 exhibits scatterplots of monthly-rms τ_i vs. monthly-mean ζ at 9 PIES sites (see map in Figure 4) during Winter-1 and Winter-2. Winter-1 exhibits significant correlation between monthly-rms τ_i and monthly-mean ζ with correlation coefficient $r = -0.465$, while Winter-2 exhibits lower, yet significant, correlation with $r = -0.236$. If the true correlation were zero, the probability is very small that an estimated correlation would randomly be -0.465 or -0.236 is respectively 0.0014% and 3.5% for Winter-1 and Winter-2. The higher magnitude correlation observed during Winter-1 may be explained by the strongly developed UWE which produces a broad negative ζ region in the UB.

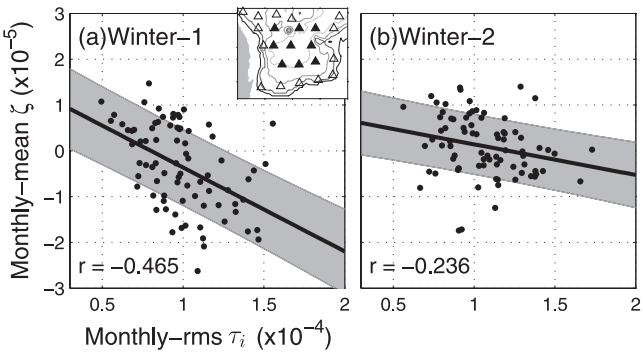

Figure 4. Scatterplots of monthly-rms τ_i vs. monthly-mean ζ at 9 PIES sites (solid triangles in map) during (a) Winter-1 and (b) Winter-2. Thick solid lines are fitted by least-squares and gray-shaded zones indicate error bounds which contain at least 50% of the predictions. The correlation coefficients are -0.465 and -0.236 for Winter-1 and Winter-2, respectively.

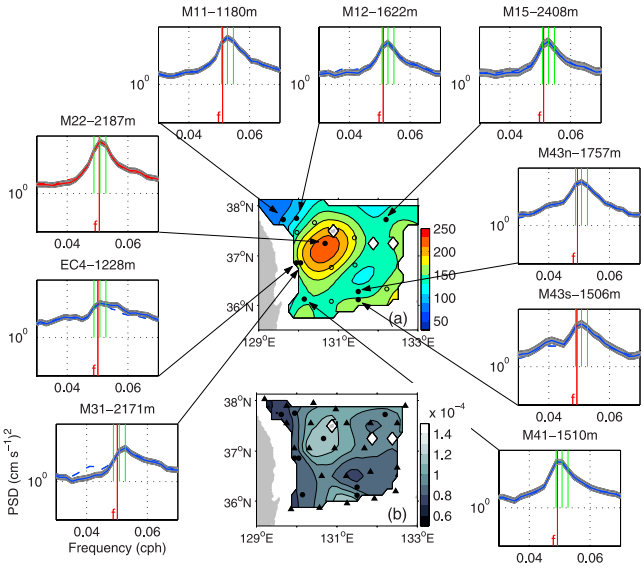

Figure 5. Power spectra for zonal (solid line) and meridional (dashed line) components at nine bottom CM sites, where the observed current records are long enough to have more than 20 segments of 512 data points (21.33 days) overlapped by 50%. Vertical red and green lines indicate the local Coriolis frequency f and three spectral estimates closest to f and the spectral peak. (a) 2-year mean map of 5°C depth (Z_5) (contour interval 20 m). (b) 2-year rms amplitude map of τ_i the band-pass filtered τ in the near-inertial frequency bands (contour interval 10^{-5} sec). Solid circles and triangles on the maps indicate bottom current meters and PIESs, respectively.

[19] Figure 5 illustrates power spectra in a band around the inertial frequency for u and v current components (solid and dashed spectral curves, respectively) observed by the deep CMs. All current spectra but one exhibit a spectral peak of near-inertial oscillations at a frequency slightly higher than the local f ($\sim$1.04f). The one exception (red spectral curve) is site M22 (2187 m depth), which exhibits the highest near-inertial spectral energy among the deep CMs.

[20] Figures 5a and 5b exhibit the mean map of the mesoscale circulation (Z_5) and the rms amplitude map of τ_i during the 2 years. Comparison of these maps with the CM locations reveals that site M22 is located near the center of the UWE, where strong near-inertial oscillations occur in the upper ocean.

4. Conclusion

[21] We observed hot spots of upper near-inertial wave energy near the UWE and near the southern and eastern edges of the observational area along the TWC branches. This is consistent with *Kunze*'s [1985] interpretation, because in such locations the f_{eff} is smaller than the local f, and those regions can trap near-inertial energy. Scatterplots of monthly-rms τ_i vs. monthly-mean ζ support this interpretation. Similar trapping of near-inertial waves has been reported at the south side of the SPF and northern part of a warm eddy along 134°E in the Japan/East Sea by *Shcherbina et al.* [2003].

[22] All deep CM sites but one exhibit a blue-shifted inertial peak ($\sim$1.04f). This is consistent with *Garrett*'s [2001] interpretation that near-inertial wave energy arrives at the ocean bottom equatorward of the source region. In the contrary, the lack of blue shifting at site M22 implies that its inertial wave energy probably originated locally. The highest near-inertial power spectrum at site M22 suggests that the UWE plays an important role in allowing the upper near-inertial energy trapped in that anticyclonic feature to drain to the deep ocean. This may be explained by a simulation result of *Lee and Niiler* [1998].

[23] *D'Asaro* [1991] suggested vertical integrating measurements as a promising approach to measure weak low-mode near-inertial waves. In that sense, this note confirms his prediction and demonstrates the instrumental capability of the PIES to detect the low-mode near-inertial waves in the ocean. By combining this with the traditional capability of a PIES array to map the mesoscale circulation, we demonstrate the impact of mesoscale circulation on the near-inertial wave energy distributions in the southwestern Japan/East Sea.

[24] **Acknowledgments.** We thank D. A. Mitchell, K. L. Tracey, and W. J. Teague for their great help in processing the PIES and CM data. This work was supported by the Office of Naval Research "Japan/East Sea DRI", including two Basic Research Programs, the Japan/East Sea initiative under grants N000149810246 and N000140410658, and the Naval Research Laboratory's "Linkages of Asian Marginal Seas" under Program Element 0601153N.

References

D'Asaro, E. A. (1985), The energy flux from the wind to near-inertial motions in the surface mixed layer, *J. Phys. Oceanogr.*, *15*, 1043–1059.

D'Asaro, E. A. (1991), A strategy for investigating and modeling internal wave sources and sinks, in *Dynamics of Oceanic Internal Gravity Waves: Proceedings of the 'Aha Huliko'a Hawaiian Winter Workshop*, edited by P. Müller and D. Henderson, pp. 451–466, Hawaii Inst. of Geophys., Honolulu.

Fu, L.-L. (1981), Observations and models of inertial waves in the deep ocean, *Rev. Geophys.*, *19*, 141–170.

Garrett, C. (2001), What is the "near-inertial" band and why is it different from the rest of the internal wave spectrum?, *J. Phys. Oceanogr.*, *31*, 962–971.

Kunze, E. (1985), Near-inertial wave propagation in geostrophic shear, *J. Phys. Oceanogr.*, *15*, 544–565.

Lee, D.-K., and P. P. Niiler (1998), The inertial chimney: The near-inertial energy drainage from the ocean surface to the deep layer, *J. Geophys. Res.*, *103*, 7579–7591.

Mitchell, D. A., J. W. Book, K.-I. Chang, M.-S. Suk, W. J. Teague, K. L. Tracey, D. R. Watts, M. Wimbush, and J.-H. Yoon (2005), Upper circulation patterns in the southwestern Japan/East Sea, *Deep Sea Res., Part II*, in press.

Niwa, Y., and T. Hibiya (1999), Response of the deep ocean internal wave field to traveling midlatitude storms as observed in long-term current measurements, *J. Geophys. Res.*, *104*, 10,981–10,989.

Park, J.-H., D. R. Watts, K. L. Tracey, and D. A. Mitchell (2005), A multi-index GEM technique and its application to the southwestern Japan/East Sea, *J. Atmos. Oceanic Technol.*, in press.

Shcherbina, A. Y., L. D. Talley, E. Firing, and P. Hacker (2003), Near-surface frontal zone trapping and deep upward propagation of internal wave energy in the Japan/East Sea, *J. Phys. Oceanogr.*, *33*, 900–912.

Teague, W. J., D. R. Watts, J. W. Book, K.-I. Chang, P. J. Hogan, D. A. Mitchell, M.-S. Suk, K. L. Tracey, M. Wimbush, and J.-H. Yoon (2005), Deep circulation in the southwestern Japan/East See, *Deep Sea Res., Part II*, in press.

Watts, D. R., and H. T. Rossby (1977), Measuring dynamic heights with inverted echo sounders: Results from MODE, *J. Phys. Oceanogr.*, *7*, 345–358.

J.-H. Park and D. R. Watts, Graduate School of Oceanography, University of Rhode Island, Narragansett, RI 02882-1197, USA. (jpark@gso.uri.edu; rwatts@gso.uri.edu)